Microscale simultaneous measurement of carbon and nitrogen isotopes on natural diamond

Akizumi Ishida (1), Kouki Kitajima (2), Ko Hashizume (3), Michael J. Spicuzza (2), Alexander Zaitsev (4, 5), Daniel J. Schulze (6), and John W. Valley (2)

(1) Department of Earth Science, Graduate School of Science, Tohoku University, Sendai 9808578, Japan
(2) WiscSIMS, Department of Geoscience, University of Wisconsin-Madison, WI 53706, USA
(3) Faculty of Science, Ibaraki University, Mito 3108512, Japan
(4) The College of Staten Island/CUNY, 2800 Victory Blvd., Staten Island, NY 10312, USA
(5) Gemological Institute of America, 50 W 47th St #800, New York, NY 10036, USA
(6) Department of Earth Sciences, University of Toronto, Mississauga, Ontario L5L 1C6, Canada

Emails:
ishidaz@tohoku.ac.jp, saburo@geology.wisc.edu, ko.hashizume.sci@vc.ibaraki.ac.jp, spicuzza@geology.wisc.edu, Alexander.Zaitsev@csi.cuny.edu, daniel.schulze@utoronto.ca, valley@geology.wisc.edu

*Corresponding author. e-mail: Akizumi Ishida (ishidaz@tohoku.ac.jp)
Phone and Fax: +81-22-795-5789

Final Published Paper:
Ishida A, Kitajima K, Hashizume K, Spicuzza MJ, Zaitsev A, Schulze DJ, and Valley JW (2023) Microscale Simultaneous Measurement of Carbon and Nitrogen Isotopes on Natural Diamond. Geostandards and Geoanalytical Research, 10 p. doi: 10.1111/ggr.12485

Keywords
Kelsey Lake Diamond, nitrogen isotope composition, carbon isotope composition, SIMS, UWD-1

Abstract

Simultaneous analysis of carbon and nitrogen isotope ratios by SIMS was applied for the first-time to a natural diamond from the Kelsey Lake kimberlite, State Line Distinct, Colorado (UWD-1). This in situ procedure is faster, reduces sample size for analysis, and measures both isotope ratios from a single ~10 μm diameter pit, a critical advantage for zoned diamonds. The carbon isotope ratio (expressed as $\delta^{13}C_{VPDB}$) of the bulk UWD-1 crystal, determined by the conventional combustion method in the present study, is -5.9‰±0.2‰ (VPDB, 2s). Nitrogen concentration ([N]) and isotope ratio (expressed as $\delta^{15}N_{Air}$) were determined by stepwise combustion and gas-source mass-spectrometry, resulting in 553±64 μg g^{-1} and -6.7‰±1.1‰ (Air, 2s), respectively. Secondary ions of $^{12}C_2^-$, $^{12}C^{13}C^-$, $^{12}C^{14}N^-$, and $^{12}C^{15}N^-$ were simultaneously measured by SIMS using three Faraday cups and one electron multiplier. The spot-to-spot reproducibility of $\delta^{13}C$ and $\delta^{15}N$ values for the UWD-1 (178 spots on 16 chips, 10 μm spots), were 0.3‰ and 1.6‰, respectively (2s). While $^{12}C^{14}N^-/^{12}C_2^-$ ratios, which are an indicator for [N], varied up to 12% among these 16 chips, such variation did not correlate with either $\delta^{13}C$ or $\delta^{15}N$ values. We propose that UWD-1 is a suitable analytical standard for microscale in-situ analysis of $\delta^{13}C$ and $\delta^{15}N$ values in diamond samples.

Introduction

Carbon and nitrogen isotope ratios (expressed as $\delta^{13}C$ and $\delta^{15}N$) in natural diamonds can constrain the formation process and environment of the diamond genesis, indicating conditions of Earth's interior. Such data are important in many disciplines including gemology and materials science, Earth science, and cosmochemistry. Reported nitrogen concentrations of natural diamonds vary from <1 to 3500 μg g^{-1}, and is the basis of classification (type-1 vs. type-2), reflecting differences in the genesis (Cartigny et al., 2014, Shirey et al., 2019). Complex growth zoning observed by cathodoluminescence (CL) imaging and correlated C and N isotope ratios provide complementary geochemical data to understand diamond growth (e.g., Bulanova *et al*. 2002, Craven *et al.*, 2009, Hauri *et al*. 2002, Palot *et al*. 2014, Petts *et al*. 2015). Microscale isotope heterogeneity in

diamond, revealed by SIMS analysis, provides new constraints on the genesis, such as subduction history of the slab or interaction with fluids (e.g., Cartigny et al., 2014, Deines et al. 1993, Thomassot et al., 2007, Palot et al., 2014). Previous reports for microscale analysis of carbon and nitrogen isotope ratio in diamond (e.g., Craven *et al.*, 2009, Gress et al., 2021, Hauri *et al*. 2002, Palot *et al*. 2014, Petts *et al*. 2015, Stern et al., 2014), have required two laterally separate analysis spots for carbon and nitrogen measurements respectively. A recent SIMS study measured $\delta^{13}C$, [N], and $\delta^{15}N$ values in the same spot, however, the $\delta^{15}N$ value was measured separately after $\delta^{13}C$ measurement (Lai et al., 2022). In this case, depth differences can be problematic. The simultaneous determination of carbon and nitrogen isotopes in one analytical spot with high precision and spatial resolution for a diamond sample has not been previously reported.

Recent improvements of microscale isotope analysis using a large-radius multicollector SIMS (IMS 1280) enables the simultaneous analysis of $\delta^{13}C$ and $\delta^{15}N$ in organic matter with high precision (2s): 0.17‰ for carbon and 0.56‰ for nitrogen isotope ratios from pits measuring 12 μm in diameter (Ishida *et al.* 2018). This method was achieved by developing a new geometry of detectors to be able to collect secondary molecular ions of $^{12}C_2^-$, $^{12}C^{13}C^-$, $^{12}C^{14}N^-$, $^{12}C^{15}N^-$, and $^{12}C_2H^-$ with a high mass resolving power of more than 8000. The mass bias of SIMS and tailing interferences were calibrated. In this method, it was confirmed that secondary ion yields of single carbon ions ($^{12}C^-$) and double carbon ions ($^{12}C_2^-$) were similar for the same reference material, anthracite (UWLA-1), indicating that $^{12}C_2^-$ ions are appropriate for analysis in material that is mainly composed of carbon. This is also proven by previous diamond research which used $^{12}C_2^-$ and $^{12}C^{14}N^-$ ions to determine nitrogen concentrations in diamond (e.g., Smart et al., 2011, Lai et al., 2022). Simultaneous detection of m/z ratios of 24, 25, 26, and 27 enabled determinations of carbon and nitrogen isotope ratios from a single spot. Such analysis is not possible with analysis of mono-atomic carbon ions. Mass spectrum peak shapes are shown in the figure 2 in Ishida et al. (2018).

In the present study, we investigated a diamond from the Kelsey Lake kimberlite, Colorado, USA, that has been used previously as a standard for carbon isotope analysis (Liu *et al*. 2009), to evaluate it as a reference material for simultaneous SIMS analysis of $\delta^{13}C$, $\delta^{15}N$, and nitrogen concentration ([N], hereafter). Two suites of diamond, peridotite-type (P-suite) and eclogite-type (E-suite) were recognized in the Kelsey Lake region (Schulze *et al*. 2008). The typical $\delta^{13}C$ value for P-suite diamonds in this region is about -

6.2‰ with variable but high [N] (approximately 1300 to 2550 μg g^{-1}). In contrast, the E-suite diamonds have more scattered $\delta^{13}C$ values ranging from -12 to -5.5‰, with [N] less than 800 μg g^{-1} (e.g., Schulze *et al*., 2008, Van Rythoven *et al*., 2017). Similar ranges in $\delta^{13}C$ values and [N] are reported by previous studies, suggesting differences in the formation model of the diamond (e.g., Cartigny *et al*. 2001, Cartigny and Marty 2013, Stachel *et al*. 2009a, Van Rythoven *et al*. 2017). The $\delta^{15}N$ values of global P-suite diamonds mostly range from -18 to +12‰ globally with some negative outliers down to -40‰, and for E-suite diamonds, $\delta^{15}N$ values mostly range from -12 to +12‰ (Cartigny *et al*. 2014). Such relatively lower values in $\delta^{15}N$ of P-suite diamond are considered to be derived from the ^{15}N-depleted primordial mantle (Cartigny and Marty 2013). Microscale analysis performed in previous studies revealed that $\delta^{13}C$ values increase from the core to rim with decreasing [N] in some natural diamonds (e.g., Bulanova *et al*. 2002, Hauri et al., 2002, Lai et al., 2022, Smart *et al*. 2011, Stachel *et al*. 2009b). Such microscale zonation in diamonds constrains models of diamond genesis and whether an oxidized or reduced fluid was responsible. Thus, simultaneous microscale analysis of $\delta^{13}C$, $\delta^{15}N$, and [N] values can in some cases provide a detailed record of the origin, formation process, and temperature-time residence history of the diamond.

Material and Methods

Sample preparation

The UWD-1 sample is part of a single crystal of diamond provided by Howard Coopersmith from the Kelsey Lake diamond mine in the State Line kimberlite distinct on the Colorado-Wyoming border, USA (Appendix Fig. S1). A 0.5 g piece of the diamond (formaly called KLD9.41) was cut by laser into a thin (1 mm thick, ~100 mg) slice, polished, and then cut into eighteen ~1 mm^3 cubes at the Gemological Institute of America (GIA). The cubes and chips from this slice constitute the UWD-1 sample. Some pieces were used for the bulk carbon isotope analysis and four of the cubes were used for the bulk measurements of $\delta^{15}N$ and [N]. For SIMS measurement, 16 chips were pressed into indium within 8 mm of the center of a 25.4 mm diameter mount at random rotations to vary the crystallographic orientation (Fig. 1). To avoid carbon and nitrogen contamination, no epoxy resin was used. There are no mineral inclusions observed in the polished face, and no clear zoning observed in CL images of examined samples (Appendix Fig. S2).

Bulk carbon and nitrogen isotope measurements of the diamond

Carbon isotope ratios were analyzed by combustion of four aliquots of UWD-1 using a gas-source mass spectrometer at the University of Wisconsin-Madison. Briefly, the 0.28 to 1.05 mg samples were combusted in an oxygen atmosphere derived from CuO in a closed silica glass tube at 950 °C overnight. Generated CO_2 was purified cryogenically and measured by Finnigan/MAT251 gas-source mass spectrometer. The long-term $\delta^{13}C_{VPDB}$ average value for NBS-21 graphite is -28.32±0.06‰ (2s, n=8) by using the same system.

The bulk nitrogen isotope analyses were performed by the Balzers QMG420 quadrupole mass spectrometer at Ibaraki University, Japan, based on the method described by Ishida et al. (2012). To determine the nitrogen isotope ratio for nitrogen concentrations at μg g^{-1} levels in carbonaceous material, surface contamination and generation of carbon monoxide are problematic and cannot be removed by a conventional method. Thus, a separate session using the stepwise combustion method is required. The platinum-wrapped sample was combusted in an oxygen atmosphere and heated in two temperature steps, at 500 °C and 1200 °C. Heating at 500 °C was performed for 30 minutes to remove surface contamination, and the main phase of the diamond was combusted at 1200 °C for 90 minutes. This analytical procedure was established by pilot analyses of an artificial diamond (see Appendix Information S3-1, Table S4). The oxygen pressure during each analysis was approximately 4.0×10^2 Pa and the nitrogen contamination associated with the oxygen was less than 2.0×10^{-11} g (<0.003% v/v of released sample N_2). The amount of carbon, converted into CO_2, was monitored during combustion, and the 1200 °C combustion was repeated 2 or 3 times until the total released amount of carbon reached 100% v/v within analytical error. Nitrogen in the diamond was released accompanied by the combustion of diamond and was finally converted into N_2 via the catalytic effect of platinum. The amount of N_2 gas was quantified manometrically in the gas extraction line and was purified cryogenically and measured by the mass spectrometer. The reproducibility of nitrogen isotope analysis, ±0.73‰, was determined by replicate measurements of working standard of N_2 gas purified from air ($\delta^{15}N_{Air}$ = -0.36‰, Appendix Table S5). Detailed procedure and standardization of working standard using international reference material are described in Appendix S3-1.

The value of $\delta^{13}C_{VPDB}$ is defined as,

$$\delta^{13}C_{VPDB} = [(^{13}C/^{12}C)_{sample}/(^{13}C/^{12}C)_{VPDB} - 1] \times 10^3 \quad (‰) \quad (1)$$

,in per mil notation, for a sample and the VPDB standard (Vienna Pee Dee Belemnite). The

values of $\delta^{15}N_{Air}$ is defined as,

$$\delta^{15}N_{Air} = [(^{15}N/^{14}N)_{sample}/(^{15}N/^{14}N)_{Air} - 1] \times 10^3 \quad (‰) \quad (2)$$

,in per mil notation for a sample and Air, the international measurement standard. The $(^{13}C/^{12}C)_{VPDB}$ ratio is defined as 1.12372×10^{-2} from the $^{13}C/^{12}C$ ratio of Pee Dee Belemnite (Craig 1957), and the $(^{15}N/^{14}N)_{Air}$ is defined as 3.6765×10^{-3} (Junk and Svec 1958).

SIMS analysis

Carbon and nitrogen isotope measurements were conducted using a CAMECA IMS 1280, a large-radius multi-collector ion microprobe, housed at the WiscSIMS Laboratory, Department of Geoscience, University of Wisconsin-Madison. The indium sample mount was degassed for more than 24 hours to attain below 1.3×10^{-5} Pa in the storage chamber of the SIMS before analysis. The primary $^{133}Cs^+$ beam with an intensity of 2.5 nA and total impact energy of 2.0×10^4 V was focused on the sample surface with a spot diameter of ~12 μm. The secondary optics and detector array were configured to match those described in Ishida *et al*. (2018). The total analysis time was ~5 minutes for one spot consisting of 60 seconds for pre-sputtering, 60 seconds for centering of secondary ions (DTFA-X, -Y), and 160 seconds (8 seconds × 20 cycles) of measurement. An electron gun and gold coating on the sample surface were used for electric charge compensation.

Secondary molecular ions of $^{12}C_2^-$, $^{12}C^{13}C^-$, and $^{12}C^{14}N^-$ were collected using three Faraday cup (FC) detectors on the positions of L'2 with 10^{10} Ω resistor, C and H1 with 10^{11} Ω resistors. The secondary molecular ions of $^{12}C^{15}N^-$ were collected by an electron multiplier (EM) on H2 position, simultaneously (see Fig. 1 and 2 in Ishida et al., 2018 for detailed analytical conditions and detector geometry). Typical count rates of these secondary ions on UWD-1 are 6.7×10^8 counts per second (cps), 1.5×10^7 cps, 2.3×10^6 cps, and 8.3×10^3 cps, respectively. The exit slit configurations were set as follows: 150μm width for the FCs on C and H1 positions and the EM on H2, and 500μm width for the FC on L'2 position (corresponding to position #3 in Ishida et al., 2018). Mass resolving power (MRP) of ~8000 was achieved with aperture settings of 30 μm for the entrance slit and 150 μm for the exit slit for both FC and EM. Potential interference ions ($^{12}C_2H^-$ next to $^{12}C^{13}C^-$, $^{13}C_2^-$ next to $^{12}C^{14}N^-$, and $^{13}C^{14}N^-$ next to $^{12}C^{15}N^-$) were clearly separated under the MRP in the present study (see Fig.2 in Ishida et al., 2018). Measured carbon and nitrogen isotope ratios ($\delta^{13}C_{Raw}$ and $\delta^{15}N_{Raw}$) are expressed in per mil notation as follows:

$$\delta^{13}C_{Raw} = 10^3 \times [(^{12}C^{13}C^-/^{12}C_2^-)_{measured} / (^{13}C/^{12}C)_{VPDB} - 1] \ (‰) \quad (3)$$

where $(^{12}C^{13}C^-/^{12}C_2^-)_{measured}$ is defined as the ratio of measured count rates of $^{12}C^{13}C^-$ and $^{12}C_2^-$.

$$\delta^{15}N_{Raw} = 10^3 \times [(^{12}C^{15}N^- / {}^{12}C^{14}N^-)_{measured} / (^{15}N/^{14}N)_{Air} - 1] \text{ (‰)} \quad (4)$$

where $(^{12}C^{15}N^-/^{12}C^{14}N^-)_{measured}$ denotes a ratio of measured count rates of $^{12}C^{15}N^-$ and $^{12}C^{14}N^-$ ions.

Tailing corrections for both carbon and nitrogen isotope compositions were evaluated, found to be insignificant and were omitted in this diamond analysis. The $^{12}C_2H^-$ ion, which was monitored for tailing correction of $^{12}C^{13}C^-$, could not be detected because the hydride ion from diamond was below the detection limit of the FC detector in the present study. For nitrogen isotopes, the tailing from $^{13}C_2^-$ next to $^{12}C^{14}N^-$ is negligibly small at MRP 8000 (Hauri et al. 2002, Ishida et al. 2018). To correct for possible tailing of the $^{13}C^{14}N^-$ ion on $^{12}C^{15}N^-$ ion, the relative intensity factor of nitrogen (RIF_N) was calculated as 1.25×10^{-5}, estimated from the peak to tail ratio of $^{12}C^{15}N^-$ (see the method in Ishida et al., 2018). Considering the maximum count rate of $^{12}C^{14}N^-$ (2.4×10^6 cps; refer to Results and Discussion section), the tailing intensity of $^{13}C^{14}N^-$ ion on $^{12}C^{15}N^-$ ion becomes less than 0.3 cps for UWD-1. This corresponds to less than 0.04‰ on measured $\delta^{15}N$ values, which is negligible compared to the analytical reproducibility expected in this method (< 0.56‰, 2s; Ishida *et al*., 2018). During SIMS measurement, UWD-1 chip number 1 was frequently measured as a bracketing running standard to check for drift.

Results and Discussion

Bulk carbon and nitrogen isotope compositions of UWD-1

Bulk carbon isotope compositions ($\delta^{13}C_{bulk}$) of UWD-1 chips ranged from -5.98 to -5.75‰ with a mean value of -5.89±0.20‰ (2s, N=4, Table 1). Bulk nitrogen concentration ([N]) and nitrogen isotope ratios ($\delta^{15}N_{bulk}$) of four aliquots of UWD-1 range from 528 to 596 μg g^{-1} and -7.4 to -6.1‰ with mean values of 553±64 μg g^{-1} and -6.7±1.1‰, respectively (2s, Table 2). The Detailed results of nitrogen isotope measurement are summarized in Appendix S3, S5 and S6.

Simultaneous measurement of $\delta^{13}C$ and $\delta^{15}N$

Results of SIMS analysis conducted during a single session are summarized in Table 3. A total of 178 spots on 16 individual chips of UWD-1 were measured. Secondary ion yields (definition of "yield" in this study is the number of secondary ions detected per

primary ion impact) for $^{12}C_2^-$ and $^{12}C^{14}N^-$ of UWD-1 range from 193 to 329 × 10^6 cps per nA ^{133}Cs (Mcps nA^{-1}, hereafter) of the primary ion beam, and 0.6 to 1.2 Mcps nA^{-1}, respectively. The $^{12}C^{14}N^-/^{12}C_2^-$ ratios range from 1.96 to 3.88 × 10^{-3}, with mean value of 3.51±0.42 × 10^{-3} (2s). The $\delta^{13}C_{Raw}$ values range from -10.4 to -9.7‰ with a mean value of -10.1±0.3‰ (2s). The $\delta^{15}N_{Raw}$ values range from -15.6 to -10.6‰ with a mean value of -12.8±1.6‰ (2s). These standard deviation values are comparable with those measured on bulk analyses of UWD-1 (±0.2‰ for carbon and ±1.1‰ for nitrogen, respectively in 2s). Bracketing analyses of chip #1 (N=46) proved that there was no systematic drift in $\delta^{13}C_{Raw}$ or $\delta^{15}N_{Raw}$ values through the session. All measured raw data are summarized in Appendix Table S7. There were no correlations between $\delta^{13}C_{Raw}$ and $\delta^{15}N_{Raw}$ values and secondary ion yields (Figs. 2 (a) to (c)). A typical cycle-by-cycle trend for the 20 cycles that comprise one spot analysis is shown in Appendix Fig. S8 (correspond to filename of 20200316@7.asc on chip #1 in Appendix Table S7). A monotonic trend with time was observed in the four measured secondary ions. By checking all cycle-by-cycle trends of examined spots on UWD-1, irregular elevation in secondary ion counts or isotope ratios, suggesting existence of included minerals, were not confirmed during analysis. Mean internal precisions, expressed as SE in the Appendix Table S7 were 0.2‰ and 1.6‰, for $\delta^{13}C_{Raw}$ and $\delta^{15}N_{Raw}$ values, respectively. As discussed by Ishida et al (2018), such internal precision of SIMS measurement does not reflect the heterogeneity with depth of the sample, however, these values were smaller or comparable with those determined reproducibility by 176 spot-by-spot analyses above.

Evaluation of UWD-1 as an analytical standard for diamond analysis by SIMS

Zoning and systematic grain-dependent differences have not been observed in UWD-1 for $\delta^{13}C_{Raw}$ and $\delta^{15}N_{Raw}$ values, and $^{12}C^{14}N^-/^{12}C_2^-$ ratios. While secondary ion yields of $^{12}C_2^-$, $^{12}C^{14}N^-$, and $^{12}C^{14}N^-/^{12}C_2^-$ ratios show wide variation, $\delta^{13}C_{Raw,}$ and $\delta^{15}N_{Raw}$ values show homogeneous distribution within stated precision of 0.3‰ and 1.6‰, respectively (2s, Figs. 2 (a) to (e)). A slightly larger variation of $\delta^{15}N_{Raw}$ was observed, however, there was no correlation between $^{12}C^{14}N^-$ yields or any other analytical factors, such as primary beam intensity and pressure in the analysis chamber (Fig. 2(b), Appendix Table S7). The $^{12}C^{14}N^-/^{12}C_2^-$ ratios, which indicate [N] at each spot, varied ±12% m/m (2s, Table 3), and also have no correlation with other analytical parameters such as topography or slight gradations seen in CL images (Appendix Fig. S2). Figures 2 (d) and (e) show plots

of $\delta^{13}C_{Raw}$ or $\delta^{15}N_{Raw}$ values against $^{12}C^{14}N^-/^{12}C_2^-$ ratios, indicating that neither $\delta^{13}C_{Raw}$ nor $\delta^{15}N_{Raw}$ values have a correlation with [N] in UWD-1. One outlier value in figures 2 (d) and (e), indicated as @42, was observed on chip #4 (corresponding to 20200316@42.asc in Appendix Table S7). The $^{12}C_2^-$ yield of this outlier spot is 300 Mcps nA^{-1}, which is similar to the average value of all examined spots. However, the $^{12}C^{14}N^-$ yield shows an anomalously low value of 0.6 Mcps nA^{-1}, (indicated in Fig. 2 (b)), indicating that the lowest $^{12}C^{14}N/^{12}C_2^-$ value, 1.96×10^{-3}, was caused by the low yield of $^{12}C^{14}N^-$. There are some other scattered points of $^{12}C_2^-$ and $^{12}C^{14}N^-$ yields in figures 2 (a) and (b), however, such data are included in the major population of $^{12}C^{14}N/^{12}C_2^-$ ratio and are not outliers in Figs. 1 (d) and (e). Thus, the spot @42 is the only irregular domain of apparently low-N diamond. It is noteworthy that $\delta^{13}C_{Raw}$ and $\delta^{15}N_{Raw}$ values of this spot do not show irregular values. We conclude that UWD-1 has intrinsic minor heterogeneity in [N], but that doesn't affect the isotope values.

In summary, the UWD-1 chips examined in the present study are homogeneous in $\delta^{13}C$ and $\delta^{15}N$ within ±0.3‰ and ±1.6‰, respectively (2s) and can be used as an analytical standard for carbon and nitrogen isotope analysis. Meanwhile, evaluation of [N] has ±12% m/m of analytical uncertainty, which is consistent with variations measured in bulk [N] (Table2, 3).

Evaluation of crystal orientation effects

Crystal orientation effects have been reported for SIMS analysis of isotope ratio in a few, mostly cubic minerals where differences in measured values are caused by channeling of primary ions within the crystal and thus correlate to crystal orientation (Huberty *et al.*, 2010, Kita *et al.* 2011). Diamond has not been tested for an orientation effect previously. Chip-to-chip differences were not distinguishable for either carbon or nitrogen isotope ratios (Table 3), suggesting that any effect was at least smaller than analytical precisions in this study where the 16 UWD-1 chips were randomly rotated. However, all chips in Figure 1 expose the same polished surface for analysis and thus not all crystallographic orientations were examined.

The possibility of orientation effect for carbon isotope ratio was further tested in a separate session with oriented crystals of diamond (Appendix Information S3-2). In this session, 4 chips from a natural 70 mg diamond (GIA-3, ISO-27, type IIa), were mounted together. SIMS analysis before cutting showed homogeneity of $\delta^{13}C$ values across one face

(±0.05‰, N=15). Three chips were cut along crystal planes of (100), (110), and (111), while the fourth was polished on a randomly selected surface. The four chips were pressed into a single indium mount (Appendix Fig. S9). The resulting, differences of average $\delta^{13}C_{Raw}$ values between the randomly mounted chip and three oriented chips were less than 0.13‰, and the total 2s of all examined chips was 0.19‰ (Appendix Table S10). These results show that an orientation effect is not detectable for carbon isotope ratios in a diamond at the 0.2‰ level.

SIMS Mass bias calibration

Mass biases (or instrumental mass fractionation: IMF) for SIMS data of both carbon (Bias(C)) and nitrogen (Bias(N)) isotope ratios were calculated against newly measured $\delta^{13}C_{bulk}$ and $\delta^{15}N_{bulk}$ values of UWD-1 based on the following equations.

$$\text{Bias(C)} = 10^3 \times (\alpha^{13}C_{SIMS} - 1) \quad (5)$$

$$\alpha^{13}C_{SIMS} = [1 + (\delta^{13}C_{Raw} / 10^3)] / [1 + (\delta^{13}C_{bulk} / 10^3)] \quad (6)$$

$$\text{Bias(N)} = 10^3 \times (\alpha^{15}N_{SIMS} - 1) \quad (7)$$

$$\alpha^{15}N_{SIMS} = [1 + (\delta^{15}N_{Raw} / 10^3)] / [1 + (\delta^{15}N_{bulk} / 10^3)] \quad (8)$$

Applying average SIMS measured $\delta^{13}C_{Raw}$ and $\delta^{15}N_{Raw}$ values, Bias(C) and Bias(N) in this study were calculated as -4.2‰ and -6.1‰, respectively. The correlation between Bias(C) and Bias(N), and hydrogen concentration, which is used to calibrate analysis of organic matter (e.g., Williford *et al*. 2016, Ishida *et al*. 2018), were not applied because hydride ions were below the detection limit on UWD-1. Mass biases determined in this study are different from those reported in previous diamond studies (< 1‰; e.g., Hauri et al., 2002, Smart et al., 2011, Stern et al., 2014). These differences are expected due to differences in type of SIMS instrument used and analytical conditions, such as secondary ion trajectory, between simultaneous and sequential methods. For this study, the errors of mass bias are calculated as ±0.4‰ and ±1.9‰ for carbon and nitrogen respectively (2s). These were propagated from results of deviations bulk isotope analysis, ±0.3‰ and ±1.0‰, and microscale analytical precision of ±0.3‰ and ±1.6‰, respectively (2s).

Homogeneity in carbon and nitrogen isotope ratios in UWD-1

With analytical uncertainty, a homogeneous isotope distribution of $\delta^{13}C$ and $\delta^{15}N$ values was confirmed by SIMS in the UWD-1 diamond. Although [N] values vary by ±12% m/m, there is no correlation with either $\delta^{13}C$ or $\delta^{15}N$ values. Inverse correlations between [N]

and $\delta^{13}C$ or $\delta^{15}N$ values corresponding to the cores and rims of single grains of diamond, were reported by previous investigators, suggesting possible differences in oxidation states of fluid during crystal growth (e.g., Bulanova *et al*. 2002, Lai *et al.*, 2022, Smart *et al*. 2011, Stachel *et al*. 2009b). In the present study, $\delta^{13}C$ or $\delta^{15}N$ values are consistent within analytical precision, ±0.3‰ and ±1.6‰, respectively (2s). Thus, there is no evidence to support a multistep growth model for UWD-1, and the slow growth model in a stable upper mantle is consistent with our results (e.g., Cartigny *et al*., 2001).

Conclusions

We report the first single-spot simultaneous measurement of $\delta^{13}C$ and $\delta^{15}N$ values and [N]. The bulk carbon and nitrogen isotope ratios of UWD-1, a natural, N-rich diamond from Kelsey Lake, were determined by conventional gas-source mass spectrometry methods and gave means of $\delta^{13}C$ = -5.9‰ and $\delta^{15}N$ = -6.7‰, with [N] of 553 μg g^{-1}. Results of SIMS analysis in a total of 178 spots on 16 chips of UWD-1 show homogeneous $\delta^{13}C$ and $\delta^{15}N$ values within 2s precisions of 0.3‰ and 1.6‰, respectively. There is no measurable orientation effect on these isotope ratios by SIMS. Although $^{12}C^{14}N/^{12}C_2^-$ ratio, an indicator of [N], varies by ±12% (2s) among different chips, there is no correlation between [N] and measured isotope ratios. The isotopically homogeneous UWD-1 can be used as a new analytical standard for simultaneous or sequential analysis of C and N isotope ratios in diamond using SIMS.

Declaration of competing interest

The authors declare that they have no known competing financial interests or personal relationships that could have appeared to influence the work reported in this paper.

Acknowledgment

The UWD-1 diamond in this study was kindly donated by Howard Coopersmith. We also thank Drs. Wuyi Wang (GIA) and Mark Newton for their contributions to the orientation effect test, and Prof. Hiroaki Ohfuji and Dr. Kohei Sasaki (Tohoku University) for their important suggestion and technical support for the stepwise combustion analysis of diamond. This research was partially supported by the JSPS KAKENHI to A.I. [JP18K13645], and [JP20H00190] to K.H. J.V. is supported by ERC (Synergy Grant # 856555). WiscSIMS is supported by NSF [EAR-2004618] and the University of

364 Wisconsin- Madison.
365
366 **References**
367 **Bulanova G.P., Pearson D.G., Hauri E.H. and Griffin B.J. (2002)**
368 Carbon and nitrogen isotope systematics within a sector-growth diamond from the Mir
369 kimberlite, Yakutia. **Chemical Geology 188**, 105-123.
370
371 **Cartigny P., Harris J.W. and Javoy M. (2001)**
372 Diamond genesis, mantle fractionations and mantle nitrogen content: a study of δ^{13}C-N
373 concentrations in diamonds. **Earth and Planetary Science Letters, 185**, 85-98.
374
375 **Cartigny P. and Marty B. (2013)**
376 Nitrogen isotopes and mantle geodynamics: The emergence of life and the atmosphere-
377 crust-mantle connection. **Elements, 9(5)**, 359-366.
378
379 **Cartigny P., Palot M., Thomassot E. and Harris J.W. (2014)**
380 Diamond Formation: A Stable Isotope Perspective. **Annual Reviews of Earth and**
381 **Planetary Science, 42**, 699-732.
382
383 **Craig H. (1957)**
384 Isotopic standards for carbon and oxygen and correlation factors for mass-spectrometric
385 analysis of carbon dioxide. **Geochimica et Cosmochimica et Acta, 12**, 133-149.
386
387 **Craven J.A., Harte B., Fisher D., and Schulze D.J. (2009)**
388 Diffusion in diamond. I. Carbon isotope mapping of natural diamond. **Mineralogical**
389 **Magazine**, **73**(2), 193-200.
390
391 **Deines P., Harris J.W., Gurney J.J. (1993)**
392 Depth-related carbon isotope and nitrogen concentration variability in the mantle below
393 the Orapa kimberlite, Botswana, Africa. **Geochimica et Cosmochimica et Acta** 57,
394 2781-2796.
395
396 **Gress M.U., Koornneef J.M., Thomassot E., Chinn I.L., van Zuilen K., Davies G.R.**

(2021)
Sm-Nd isochron ages coupled with C-N isotope data of eclogitic diamonds from Jwaneng, Botswana. **Geochimica et Cosmochimica et Acta** 293, 1-17.

Hauri E.H., Wang J., Pearson D.G. and Bulanove G.P. (2002)
Microanalysis of $\delta^{13}C$, $\delta^{15}N$, and N abundances in diamonds by secondary ion mass spectrometry. **Chemical Geology 185**, 149-163.

Huberty J.M., Kita N.T., Kozdon R., Heck P.R., Fournelle J.H., Spicuzza M.J., Xu H., Valley J.W. (2010)
Crystal Orientation Effects on Instrumental Bias of $\delta^{18}O$ in Magnetite by SIMS, **Chemical Geology,** 276, 269-283.

Ishida A., Hashizume K. and Kakegawa T. (2012)
Stepwise combustion analyses of distinct nitrogen isotopic compositions on Paleoproterozoic organic matter, **Geochemical Journal, 46,** 249-253.

Ishida A., Kitajima K., Williford K.H., Tuite M.L., Kakegawa T. and Valley J.W. (2018)
Simultaneous in situ analysis of carbon and nitrogen isotope ratios in organic matter by secondary ion mass spectrometry. **Geostandards and Geoanalytical Research, 45**, 97-119.

Junk G. and Svec H. (1958)
The absolute abundance of the nitrogen isotopes in the atmosphere and compressed gas from various sources. **Geochimica et Cosmochimica Acta, 14**, 234-243.

Koga K.T., Van Orman J.A. and Walter M.J. (2003)
Diffusive relaxation of carbon and nitrogen isotope heterogeneity in diamond: a new thermometer. **Physics of the Earth and Planetary interiors, 139**, 35-43.

Lai M.Y., Stachel T., Stern R.A., Hardman M.F., Pearson D.G. and Harris J.W. (2022)

Formation of mixed paragenesis diamonds during multistage growth – Constraints from in situ $\delta^{13}C$–$\delta^{15}N$–[N] analyses of Koidu diamonds. **Geochimica et Cosmochimica Acta, 323**, 20-39.

Liu Y., Taylor L.A., Sarbadhikari A., Valley J.W., Ushikubo T., Spicuzza M.J., Kita N., Ketchum R., Carlson W., Shatsky V. and Sobolev N.V. (2009)
Metasomatic origin of diamonds in the world's largest diamondiferous eclogite. **Lithos, 261**, 140-154.

Palot M., Pearson D.G., Stern R.A., Stachel T. and Harris J.W. (2014)
Isotopic constraints on the nature and circulation of deep mantle C-H-O-N fluid: Carbon and nitrogen systematics within ultra-deep diamonds from Kankan (Guinea). **Geochimica et Cosmochimica Acta, 139**, 26-46.

Petts D.C., Chacko T., Stachel T., Stern R.A. and Heaman L.M. (2015)
A nitrogen isotope fractionation factor between diamond and its parental fluid derived from detailed SIMS analysis of a gem diamond and theoretical calculations. **Chemical Geology 410**, 188-200.

Pinti D., Ishida A., Takahata N., Sano Y., Bureau H. and Cartigny P. (2016)
Micron-scale $\delta^{13}C$ determination by NanoSIMS in a Juina diamond with a carbonate inclusion. **Geochemical Journal, 50** e7-12.

Schulze D.J., Coopersmith H.G., Harte B. and Pizzolato L.A. (2008)
Mineral inclusions in diamonds from Kelsey Lake Mine, Colorado, USA: Depleted Archean mantle beneath the Proterozoic. **Geochimica et Cosmochimica Acta 72**, 1685-1695.

Schulze D.J., Harte B., E.I.M.F., Page F.Z., Valley J.W., Channer D.M.D.R. and Jaques A.L. (2013)
Anticorrelation between low $\delta^{13}C$ of eclogitic diamonds and high $\delta^{18}O$ of their coesite and garnet inclusions requires a subduction origin. **Geology, 41**, 455-458.

Shirey S.B., Smit K.V., Pearson D.G., Walter M.J., Aulbach S., et al. (2019)
Diamonds and the mantle geodynamics of carbon. In **Deep Carbon: Past to Present** (eds Orcutt B.N., Daniel I., Dasgupta R.), Cambridge Univ. Press, pp. 89–128.

Smart K.A., Chacko T., Stachel T., Muehlenbachs K., Stern R.A. and Heaman L.M. (2011)
Diamond growth from oxidized carbon sources beneath the Northern Slave Craton, Canada: A $\delta^{13}C$–N study of eclogite-hosted diamonds from the Jericho kimberlite. **Geochimica et Cosmochimica Acta, 75**, 6027-6047.

Stachel T. and Harris J. W. (2009a)
Formation of diamond in the Earth's mantle. **Journal of Physics: Condensed Matter 21**, 364206.

Stachel T., Harris J. W. and Muehlenbachs K. (2009b)
Sources of carbon in inclusion bearing diamonds. **Lithos 112S**, 625–637.

Stern R. A., Palot M., Howell D., Stachel T., Pearson D.G., Cartigny P., and Oh A. (2014)
Methods and Reference Materials for SIMS Diamond C- and N-isotope Analysis. **Canadian Centre for Isotopic Microanalysis Research Report 14-01.**

Thomassot E., Cartigny P., Harris J.W., Viljoen K.S. (2007)
Methane-related diamond crystallization in the Earth's mantle: Stable isotope evidences from a single diamond-bearing xenolith. **Earth and Planetary Science Letters** 257. 362-371.

Van Rythoven A.D., Schulze D.J., Hauri E.H., Wang J. and Shirey S. (2017)
Intra-crystal co-variations of carbon isotopes and nitrogen contents in diamond from three North American cratons. **Chemical Geology, 467**, 12-29.

Williford K.H., Ushikubo T., Lepot K., Kitajima K., Hallmann C., Spicuzza M.J., Kozdon R., Eigenbrode J.L., Summons R.E. and Valley J.W. (2016)

Carbon and sulfur isotopic signatures of ancient life and environment at the microbial scale: Neoarchean shales and carbonates. **Geobiology, 14,** 105-128.

Figure and Table captions

Figure 1.

Image of randomly rotated UWD-1 chips in an indium mount. The larger central grain is a synthetic diamond for ion beam test and tuning. Each UWD-1 chip is numbered, and SIMS analysis spots are shown by circle symbols. Scale bar indicates 3 mm. (b) Enlarged view of chip #1 (squared area in (a)). The size of SIMS analysis spots is not actual size (~12 μm).

Figure 2.

Plots of (a) $\delta^{13}C_{Raw}$ values vs. $^{12}C_2^-$ yields, (b) $\delta^{15}N_{Raw}$ values vs. $^{12}C^{14}N^-$ yields, (c) $\delta^{13}C_{Raw}$ values vs. $\delta^{15}N_{Raw}$ values, (d) $\delta^{13}C_{Raw}$ values vs. $^{12}C^{14}N/^{12}C_2^-$ ratios, and $\delta^{15}N_{Raw}$ values vs. $^{12}C^{14}N/^{12}C_2^-$ ratios. Error bars on each plot, indicating internal precision during one spot analysis (Appendix Table S7), were omitted to show plots clearly. Mean values for precisions are 0.2‰ and 1.6‰, for $\delta^{13}C_{Raw}$ and $\delta^{15}N_{Raw}$ values, respectively. There is no correlation among these values. Distributions of $\delta^{13}C_{Raw}$ and $\delta^{15}N_{Raw}$ values are shown together in the Figure 2 (c) (gray histograms on each axis). On (b), (d), and (e), an anomalous spot of 20200316@42.asc in Appendix Table S7 is shown as @42 with arrows.

Tables

Table 1

Bulk $\delta^{13}C_{PDB}$ values of four UWD-1 aliquots measured by combustion and gas-source mass spectrometry.

Table 2.

Bulk $\delta^{15}N_{Air}$ values of four UWD-1 aliquots measured by combustion and gas-source mass spectrometry.

Table 3.

Summary of 178 SIMS analyses of 16 UWD-1 chips.

Supporting materials

Appendix Figure S1

Original polished slab of UWD-1 broken into two pieces before cutting into ~ 1-mm cubes. Scale bar is 1 mm.

Appendix Figure S2

Cathodoluminescence images of measured chips of UWD-1. Each number corresponds to the chip number in Fig. 1. There is no clear zoning in any chips. Chips number #3, #9, #11, and #16 are absent because these were used for bulk $\delta^{15}N$ measurement. Scale bar is 0.5 mm.

Appendix Information S3

S3-1. Results of supportive measurements of bulk $\delta^{15}N$ value of UWD-1.

S3-2. Evaluation of crystal orientation effect of diamond using synthetic diamond. Original data summarized in Appendix Table S10.

Appendix Table S4

Combustion profile of pilot measurement of synthetic yellow diamond from ANCO Industrial Diamond Corp.

Appendix Table S5

Reproducibility of $\delta^{15}N$ values of standard air gas analysis of nitrogen isotope ratio by stepwise combustion method.

Appendix Table S6

Combustion profiles of measured four chips of UWD-1 diamond.

Appendix Table S7

Table of all SIMS analytical data for simultaneous analysis of $\delta^{13}C$, $\delta^{15}N$, and [N]. Analyses of chip #1 were used as a running standard to bracket sample analyses.

Appendix Figure S8

Typical cycle-by-cycle trends for a single spot analysis: UWD-1 (file name: 20200316@7 on UWD-1 chip 1, in Appendix Table S10).

Appendix Figure S9

(a) Chips of diamond GIA-3 mounted together in indium to test for a possible orientation effect of SIMS analysis of carbon isotope ratio in diamond. Chips cut along crystal planes of (100), (110), and (111), and a randomly cut chip are shown. Scale bar is 1.0 mm. (b) Enlarged view of randomly oriented chip. Numbers with @ marks correspond to analysis numbers by SIMS summarized in Appendix Table S10.

Appendix Table S10

Table of all SIMS analytical data in the session to evaluate orientation effects for measurement of carbon isotope ratios.

Appendix Table S11

The consumption rate of oxygen during three repeated 90-minutes combustion cycles of UWD-1 (#3) at 1200 °C. The 1200 °C step was repeated 3 times until the released amount of carbon reached 100% v/v.

Appendix Figure S12

Plot of oxygen consumption rate during three repeated measurements at 1200 °C of UWD-1 (#3). Legends of circle, square, and triangle correspond to oxygen consumption rates of the first, second, and third heating at 1200 °C. Data are summarized in Appendix Table S11.

Appendix Information S3

Supportive measurements of the present study.

S3-1. Evaluation of bulk nitrogen isotope ratios of UWD-1 by stepwise combustion method

Pilot measurement of industrial diamond

The nitrogen isotope ratio ($\delta^{15}N$) of bulk UWD-1 sample was analyzed using Balzers QMG420 quadrupole mass spectrometer housed at Ibaraki University, Japan, following the method described by Yamamoto et al. (1998) and Ishida et al. (2012). Four chips (< 0.9 mm^3 each, ~ 2.1 mg) were prepared from the same slab which was used for bulk $\delta^{13}C$ measurement. To investigate the temperature-dependent combustion profile of diamond, pilot measurements were performed using pale yellow industrial diamonds (~1.0 mm diameter) provided by ANCO Industrial Diamond Corporation. Approximately 0.7 mg of a crushed diamond particle was wrapped in platinum foil, loaded in the measurement line and was combusted in ~4.0×10^2 Pa of oxygen atmosphere. Combustions were performed in 100°C steps from 200 to 1200 °C. The 1200 °C step was repeated to confirm the complete combustion of carbon. Results are summarized in Appendix Table S4. The combustion profile shows three pieces of important information. First, below 500 °C, only a minor amount of carbon, less than 0.35% m/m of total carbon, was released suggesting that intrinsic carbon of diamond was not oxidized and released below 500 °C. Second, at 200 °C, surface contamination of carbon and nitrogen was released. Thus, it turned out combustion at 500°C is necessary to release contamination nitrogen without combustion of diamond, and isotope measurement could be omitted. We treat this step as "precombustion" hereafter. Third, the major release of carbon as CO_2 began at 600 °C and ceased at 1100 °C. This is consistent with the previous report of diamond combustion experiments in an oxygen atmosphere (Javoy et al., 1984). Major release of nitrogen occurred in the temperature range from 700 to 1100 °C. Thus, we determined the bulk analysis procedure of diamond as two-step combustion, 500 °C of precombustion and 1200 °C of the main combustion. To confirm the complete combustion of diamond, the experimental duration at 1200 °C step was set as 90 minutes, and this step was repeated until the total released amount of carbon is 100 % v/v.

Reproducibility of $\delta^{15}N$ measurement

Reproducibility of $\delta^{15}N$ values in the stepwise combustion method was determined by repeated analysis of standard air gas (STD-N), which has collected and purified from atmosphere in Ibaraki, Japan, having $\delta^{15}N$ = -0.36 ‰. Its $\delta^{15}N$ value was calibrated by measuring the working standard of iron nitride (Fe_4N, Kojundo Chemical Laboratory Co. Ltd.) which $\delta^{15}N$ value was determined by gas-source EA-IRMS as -6.4±0.2‰ (standardized by commercial stable isotope standard of L-Alanine having $\delta^{15}N_{Air}$ = 1.79±0.2‰, which was calibrated against IAEA-N-1 and -N-2 (+0.4‰ and +20.3‰) by Shoko Science Co. Ltd.). A total of 30 pipettes of STD-N were measured before, between, and after every 4 chips of UWD-1 sample measurement. The two standard deviations (2s) of STD-N throughout the different sessions was 1.46 ‰ (Appendix Table S5). The reproducibility of nitrogen concentration measurement in this system is also determined as approximately ±8%. Blank nitrogen levels associated with the gas-extraction system ranges from < 0.001×10^{-9} g at < 900 °C, to 0.03×10^{-9} g at 1200 °C. The detection limits for CO_2 pressures on this analytical line are 1.3×10^{-8} g.

The bulk $\delta^{15}N$ measurement of UWD-1

Measurements of UWD-1 chips consisted of 30 minutes of precombustion at 500 °C, and 90 minutes of main combustions at 1200 °C in 4.0×10^2 Pa of oxygen atmosphere. Any gas evolved at 500 °C was discarded because this fraction contains surface contamination. The quantification of carbon was manometrically measured by CO_2 that was cryogenically trapped during sample combustion. The 1200 °C combustion step was repeated until the total released amount of carbon reached 100 % v/v. Oxygen consumption rates (Pa min^{-1}) were measured every few minutes and are summarized in Appendix Table S11 (sample ID: UWD-1 #3). The maximum peak of oxygen consumption rate for the 1200 °C combustion appeared at around 20 minutes from the combustion start (Appendix Fig. S12). This peak at around 14 minutes appeared again in the second 1200 °C combustion on the same sample. To our knowledge, such trends have not been studied in previous diamond combustion experiments. We tentatively concluded that this trend resulted from a combination of reactions of graphitization of diamond under high temperature, oxidation of graphite, and oxidation of diamond in an oxygen atmosphere. There are many previous studies about the phase transition of graphite to diamond under anoxic high pressure, but no other studies with a similar condition to this

study (e.g., Aleksenski et al. 1997, Bundy et al. 1961, Ohfuji et al. 2010, Qian et al. 2004). Further study is needed to investigate this possibility.

Results of nitrogen and carbon concentrations and $\delta^{15}N$ values of four UWD-1 chips are summarized in Appendix Table S6. The $\delta^{15}N$ values ranged from -7.4 to -6.1 ‰, with nitrogen concentrations of 528 to 596 μg g^{-1} among the four chips. The bulk $\delta^{15}N_{Air}$ value and nitrogen concentration of UWD-1 were determined adopting average values of those analyses: -6.7±1.1‰ and 553±64 μg g^{-1}, respectively (2s).

S3-2. Evaluation of orientation effect on diamond

A separate analysis session was designed to evaluate any possible crystal orientation effect (Huberty et al., 2010; Kita et al., 2011) of carbon isotope ratios in diamond by SIMS analysis, which has not been tested previously. In this session, a nitrogen-poor diamond (GIA-3, ISO-27) that is homogeneous in $\delta^{13}C$ was selected to test the intrinsic effect of the crystal structure of diamond on measured SIMS data. Three chips were prepared laser-cut along with crystal planes of (100), (110), and (111), and one other chip was randomly cut without considering orientation. These four chips were mounted in the same indium mount (Appendix Fig. S9). Analytical conditions of SIMS and definitions of carbon isotope ratio in permil notation were the same as those described in the material and methods section in the main text.

Measured values are summarized in the Appendix Table S10. The $\delta^{13}C_{Raw}$ values measured on the "random" chip ranged -26.07 to -25.85 ‰ with a mean value of -25.93±0.15 ‰ (2s, N=9). Mean $\delta^{13}C_{Raw}$ values of three crystals with specific planes cut were -26.00‰ (N=5), -25.98‰ (N=4), and -26.06‰ (N=4) corresponding to planes of (111), (100), and (110), respectively. Thus, differences in mean $\delta^{13}C_{Raw}$ values of diamonds against "random" chip values were smaller than 2s measured on the "random" chip. The variation of all 22 spots measured on 4 chips was ±0.19 ‰ (2s). These results indicate that any orientation effect is below detection in this study for carbon isotope ratios in a diamond. Orientation effect of nitrogen isotope ratios could not be tested because nitrogen concentration is too low to evaluate isotope homogeneity smaller than reproducibility.

Appendix references

684 **Aleksenskii A.E., Baidakova M.V., Ya Vul' A., Davydov V.Y. and Pevtsova Y. A.**
685 **(1997)**
686 Diamond-graphite phase transition in ultradisperse-diamond clusters. **Physics of the**
687 **Solid State. 39**, 1007-1015.
688
689 **Bundy F.P., Bovebkerk H.P., Strong H.M. and Wentorf R.H. (1961)**
690 Diamond-graphite equilibrium line from growth and graphitization of diamond. **Journal**
691 **of Chemical Physics. 35**, 383-391.
692
693 **Huberty J.M., Kita N.T., Kozdon R., Heck P.R., Fournelle J.H., Spicuzza M.J., Xu**
694 **H. and Valley J.W. (2010)**
695 Crystal Orientation Effects on Instrumental Bias of $\delta^{18}O$ in Magnetite by SIMS.
696 **Chemical Geology, 276**, 269-283.
697
698 **Ishida A., Hashizume K. and Kakegawa T. (2012)**
699 Stepwise combustion analyses of distinct nitrogen isotopic compositions on
700 Paleoproterozoic organic matter. **Geochemical Journal, 46,** 249-253.
701
702 **Javoy M., Pineau F. and Demaiffe D. (1984)**
703 Nitrogen and carbon isotopic composition in the diamonds of Mbuji Mayi (Zaire). **Earth**
704 **and Planetary Science Letters, 68**, 399-412.
705
706 **Kita N.T., Huberty J.M., Kozdon R., Beard B.L. and Valley J.W. (2011)**
707 High precision SIMS oxygen, sulfur and iron stable isotope analyses of geological
708 materials: Accuracy, surface topography and crystal orientation. **SIMS XVII**
709 **Proceedings, Surface and Interface Analysis**, 43, 427-431.
710
711 **Ohfuji, T. Okuchi H., Odake S., Kagi H., Sumiya H. and Irifune T. (2010)**
712 Micro-/nonstructural investigation of laser-cut surfaces of single- and polycrystalline
713 diamonds. **Diamond and Related Materials, 19**, 1040-1051.
714
715 **Qian J., Pantea C., Huang J., Zerda T.W. and Zhao Y. (2004)**

716 Graphitization of diamond powders of different sizes at high pressure-high temperature.
717 **Carbon, 42**, 2691-2697.
718
719 **Yamamoto T., Hashizume K., Matsuda J. and Kase T. (1998)**
720 Multiple nitrogen isotopic compositions coexisting in ureilites. **Meteoritics and**
721 **Planetary Science, 33**, 857-870.
722

723

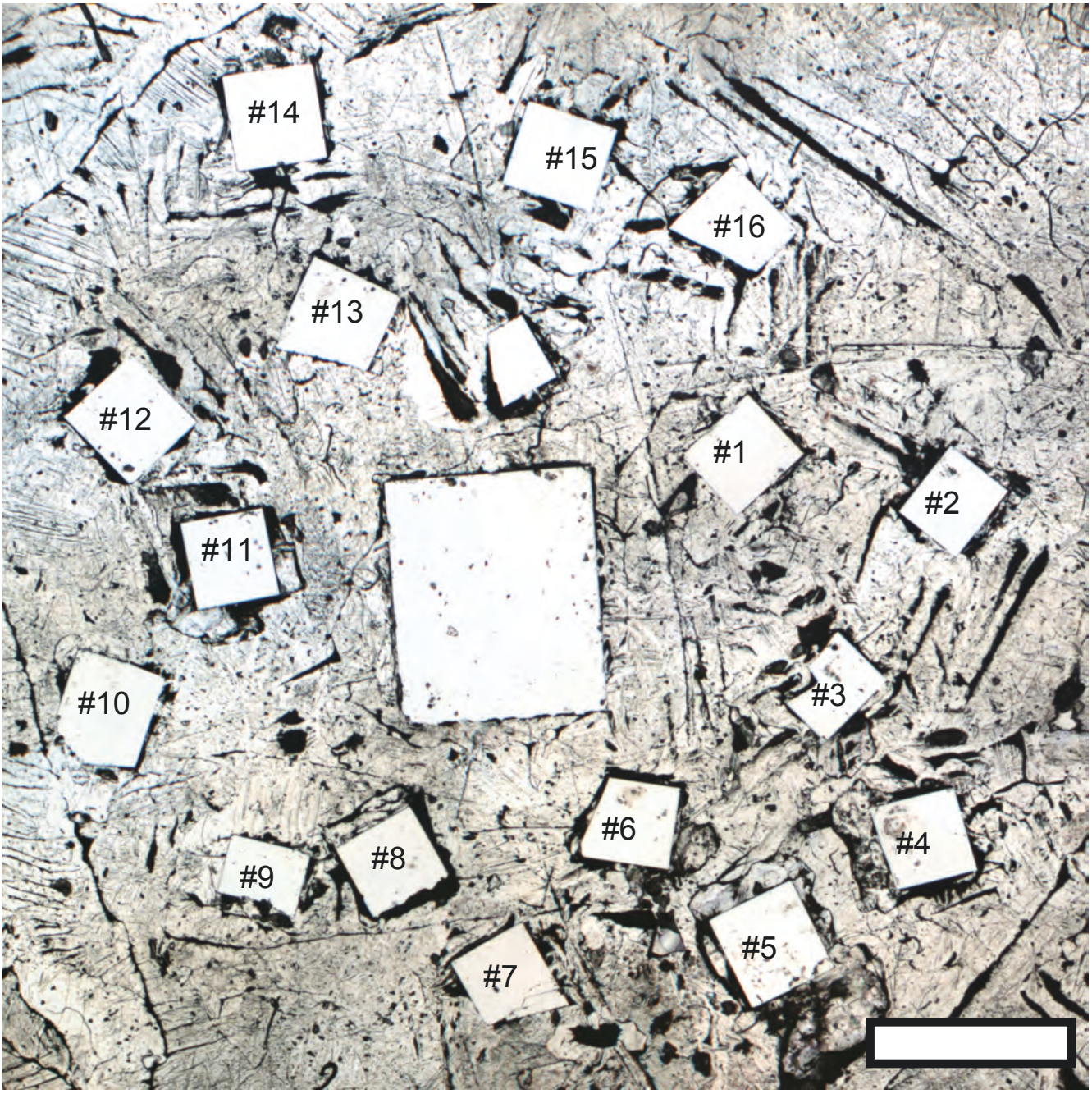

Figure 1 (Ishida et al., 2022)

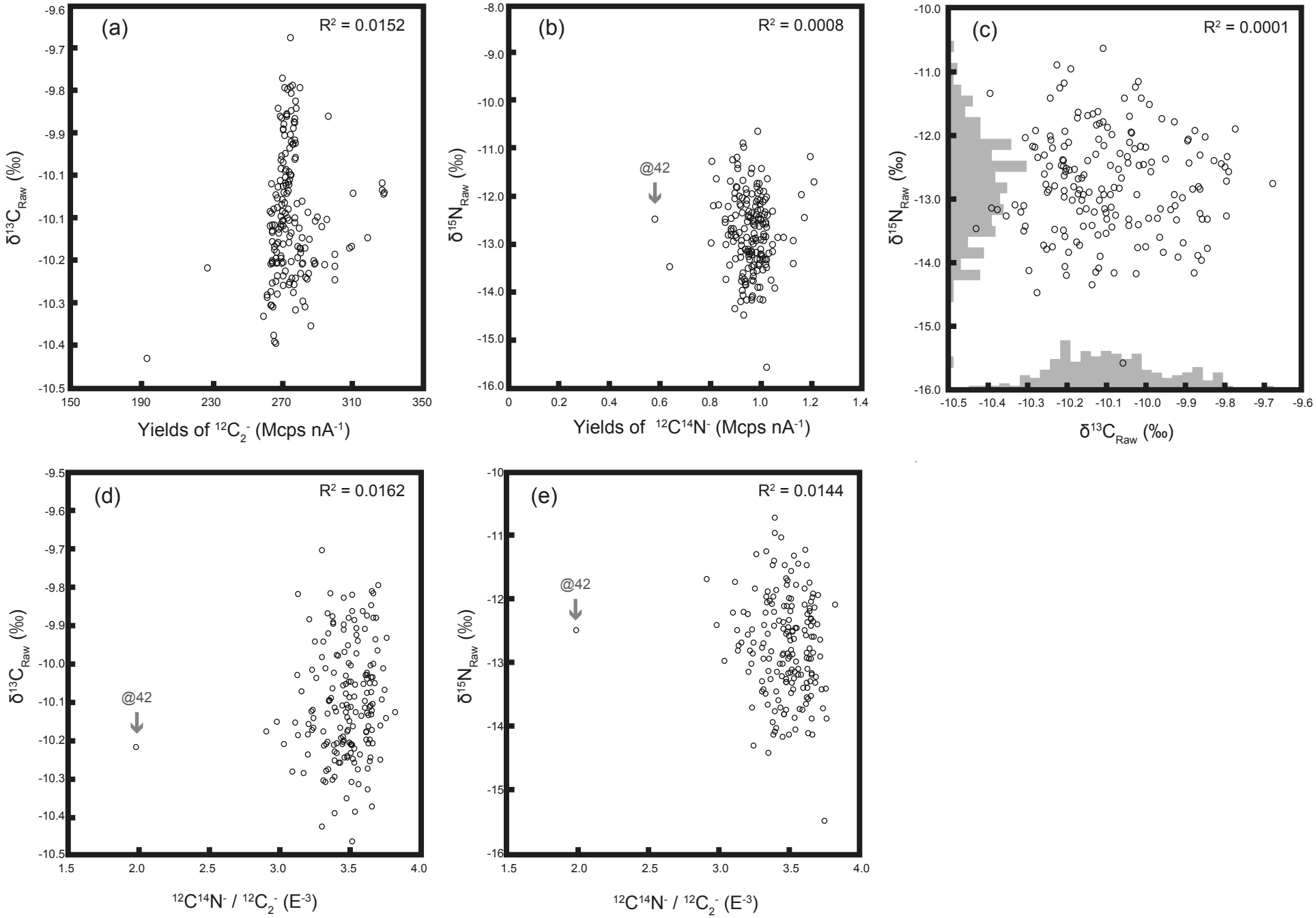

Figure 2 (Ishida et al., 2022)

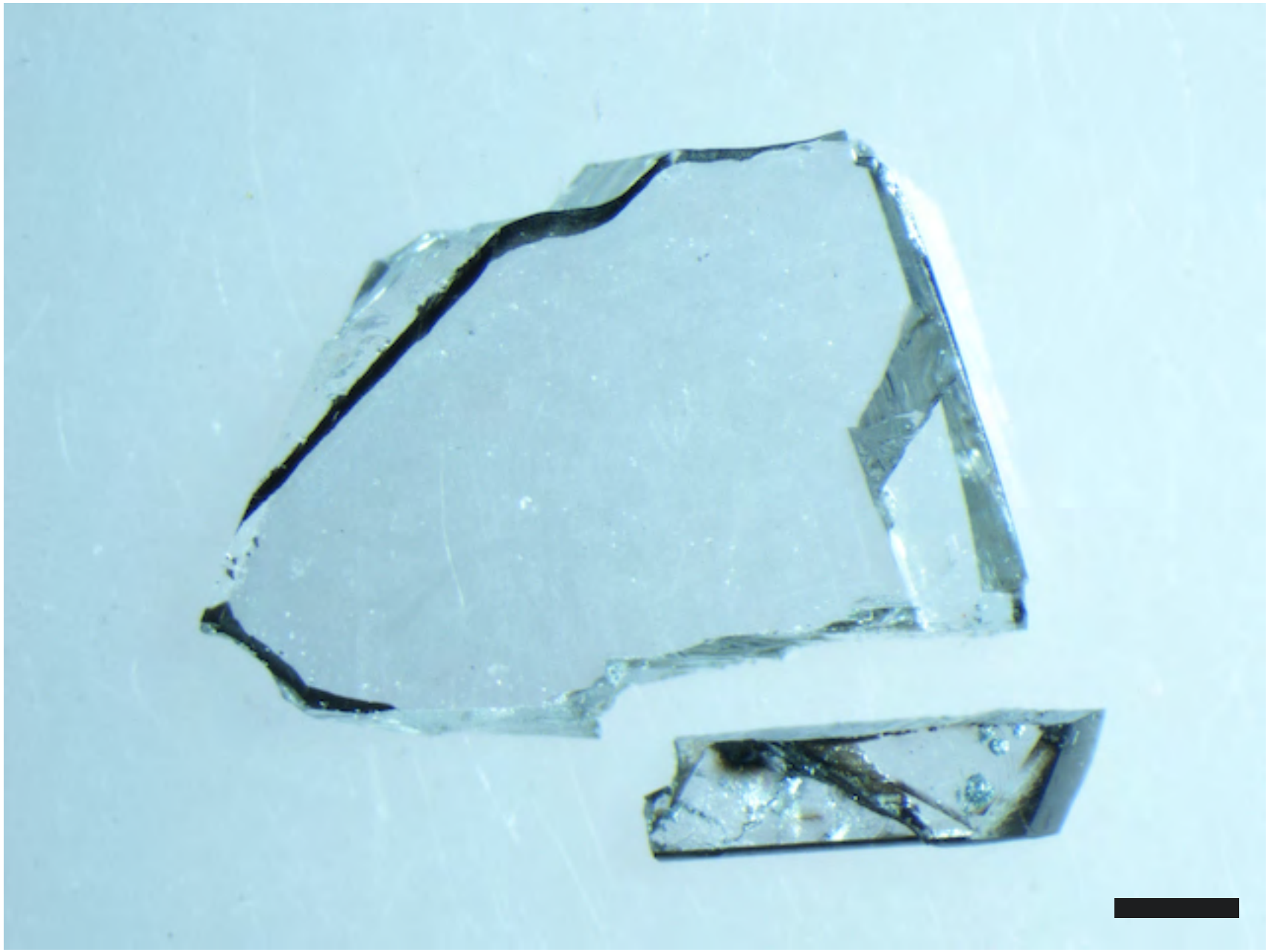

Appendix Figure S1 (Ishida et al., 2022)

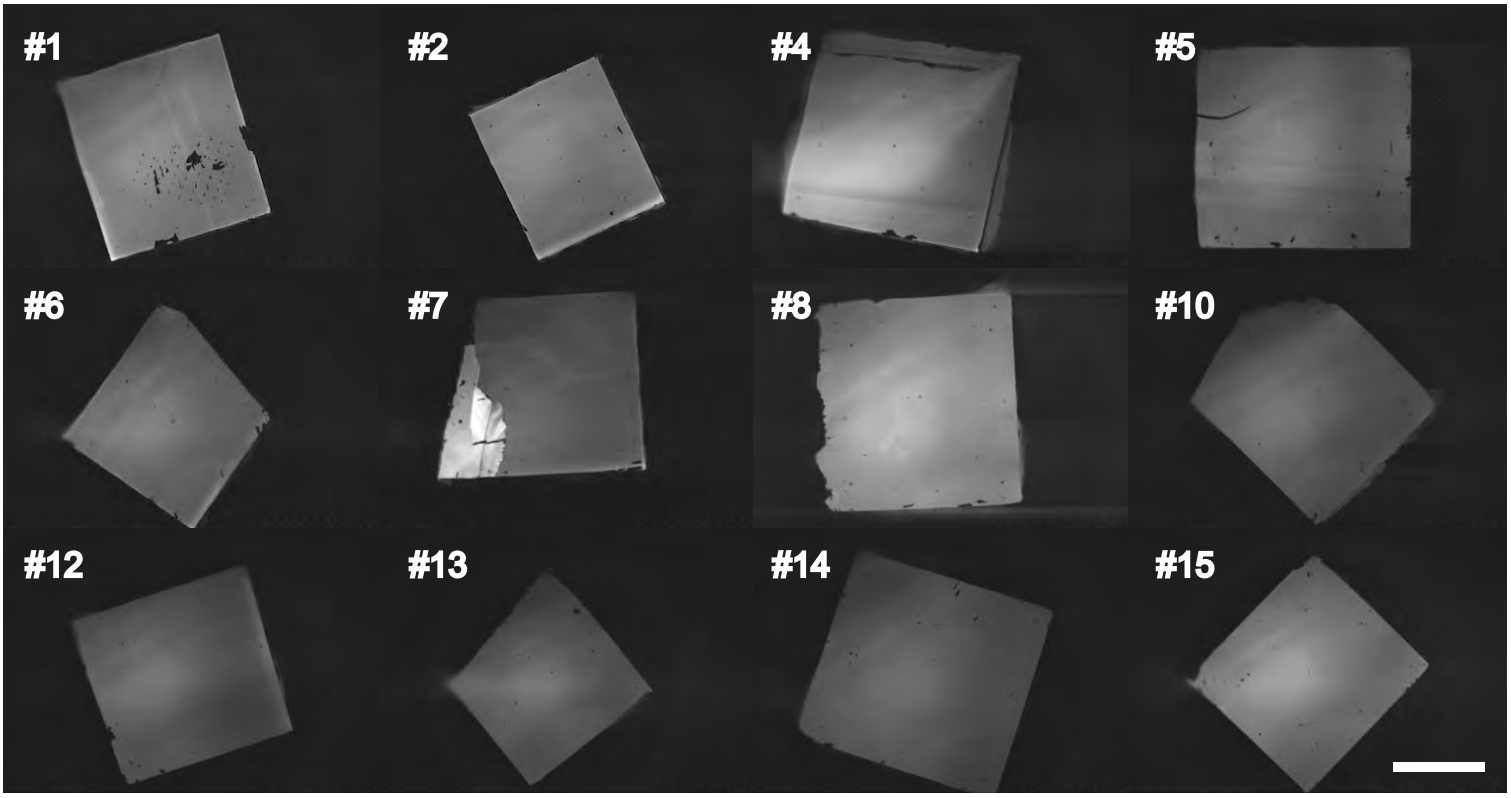

Appendix Figure S2 (Ishida et al., 2022)

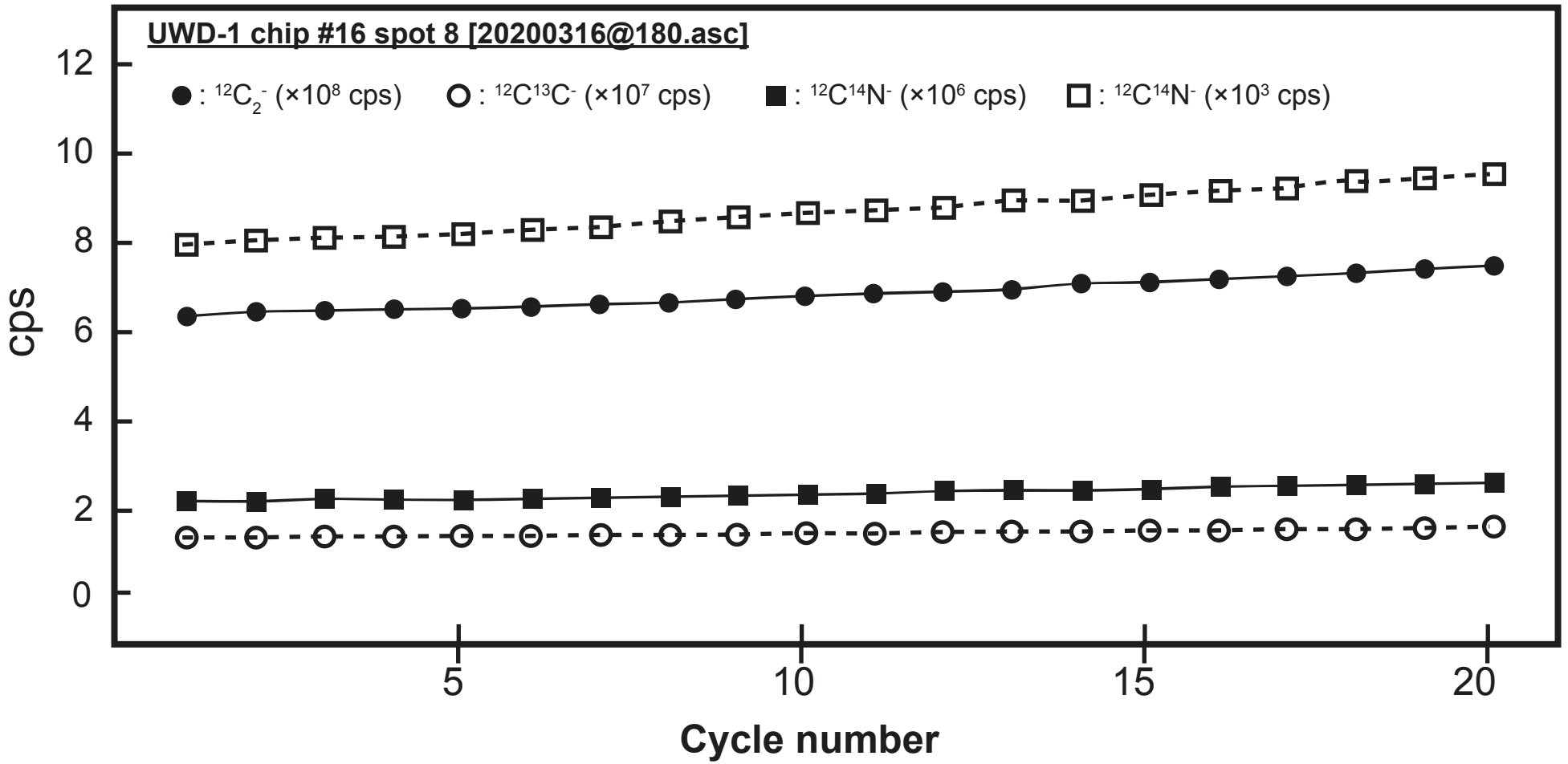

Appendix S8 (Ishida et al., 2022)

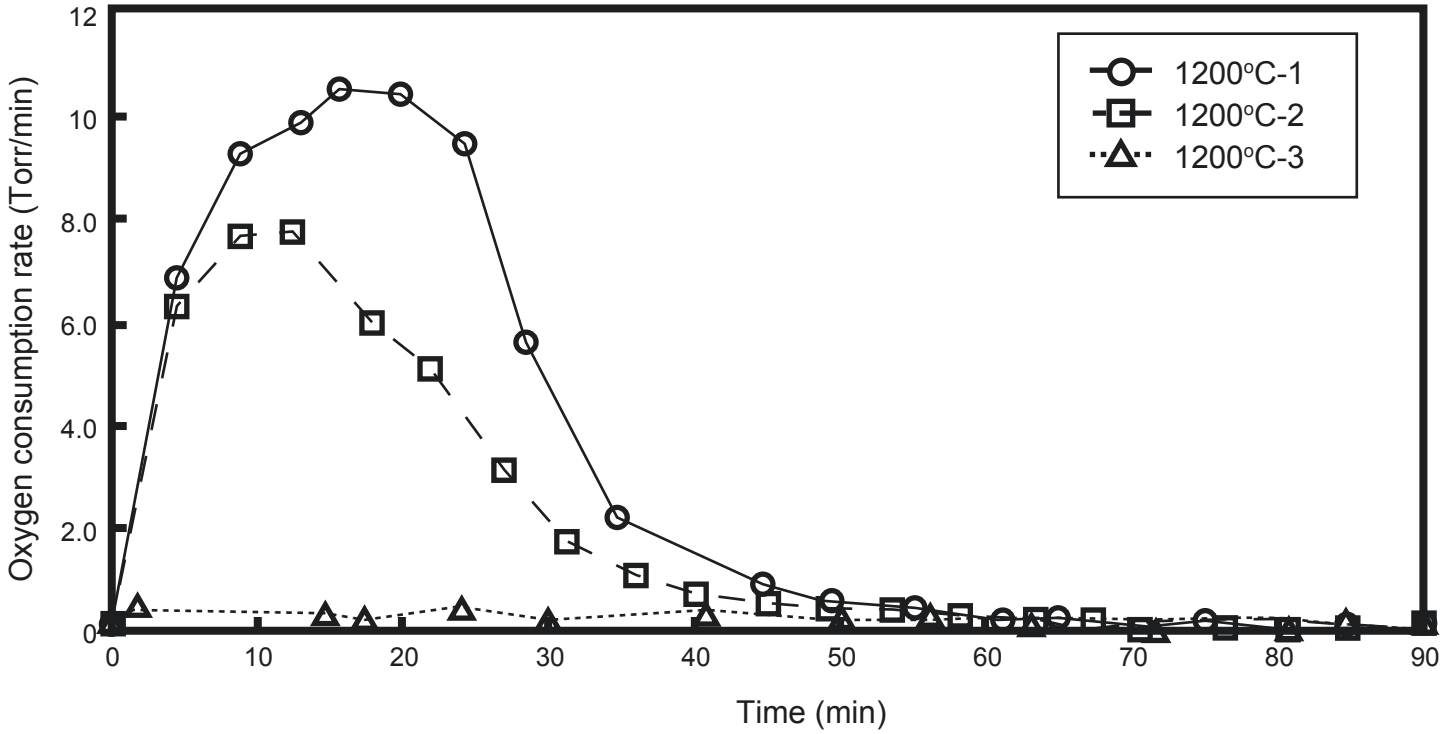

Appendix Figure S12 (Ishida et a., 2022)

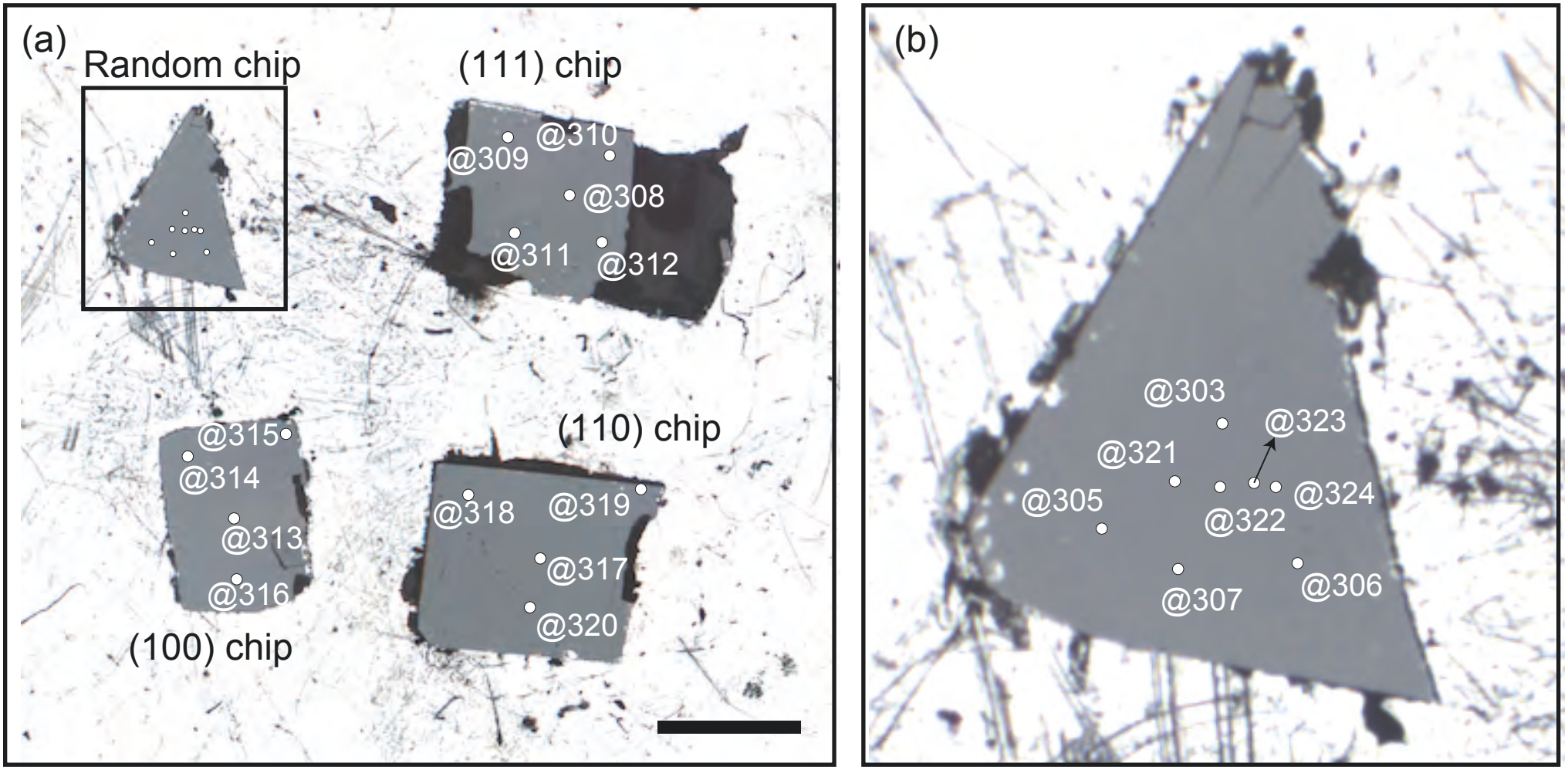

Appendix Figure S9 (Ishida et al., 2022)